STRUCTURAL CONTROL AND HEALTH MONITORING
Struct. Control Health Monit. 2016; **00**:1–20
Published online in Wiley InterScience (www.interscience.wiley.com). DOI: 10.1002/stc

Optimal design of double-skin façades as vibration absorbers

Giovanni Pipitone, Giorgio Barone*† and Alessandro Palmeri‡

School of Civil and Building Engineering, Sir Frank Gibb Building, Loughborough University, Loughborough, LE11 3RN, United Kingdom

SUMMARY

In this paper, several layouts of double skin façades (DSF) used as mass dampers to reduce the vibrations in structures under seismic events are discussed. Firstly, the mathematical coupled problem is studied considering a non-classically damped system excited by a set of accelerogram records. The design problem aims to determine the optimal values of four parameters, namely the flexural stiffness and damping of the DSF panel and the stiffnesses of the elements that connect the DSF to the primary structure. Secondly, four objective functions are presented. Two of these functions aim to minimise respectively the displacements and the accelerations of the primary structure for each earthquake. The remaining two, instead, minimise the average of the displacements and accelerations calculated for all the accelerograms given. Finally, numerical analysis are performed on a six-storey building and four DSF designs are proposed. The Particle Swarm Optimisation (PSO) is used to estimate the optimal parameters. Comparisons among the DSF layouts are presented in terms of minima of the objective functions and in terms of the power transfer functions. Moreover, a simplified design method for the connection elements is discussed. Copyright © 2016 John Wiley & Sons, Ltd.

Received ...

KEY WORDS: Earthquake engineering; Double skin façades; Non-classically damped structures; Structural optimisation; Passive control.

1. INTRODUCTION

Due to the growing population density in large cities, the number of tall buildings is continuously increasing in both low- and high-income countries, and innovations are sought to improve their performance and gain efficiency in their construction. The inherent slenderness of high-rise buildings, combined with the use of lightweight materials to reduce the dead loads, means that these structures tend to be prone to the effects of dynamic loads, such as earthquakes and windstorms.

Structural control deals with technical solutions able to mitigate the effects of vibrations in engineering structures, typically by increasing their damping capacity. Depending on the specific characteristics of structure and dynamic loads, this can be achieved with four different control strategies, namely passive, active, semi-active and hybrid control [1], which often are tailored to the specific dynamic characteristics of the structure. A dynamic vibration absorber (DVA) is an example of passive control device, consisting of a mass-damping-spring system attachment, whose natural frequency is conveniently tuned to the fundamental frequency of the main structure, with the aim of minimising the vibration amplitude in the latter [2]. Closed-form tuning criteria for the

*Correspondence to: Dr. Giorgio Barone, School of Civil and Building Engineering, Sir Frank Gibb Building, Loughborough University, Loughborough, LE11 3RN, United Kingdom
†E-mail: G.Barone@Lboro.ac.uk
‡E-mail: A.Palmeri@Lboro.ac.uk, Dynamics.Structures@Gmail.com

design of the mechanical parameters of single DVAs exist in literature for selected deterministic and broadband stochastic excitations [3–5], while numerical optimisation techniques are normally used for distributed multiple absorbers [6, 7].

A control strategy based on the use of double skin façades (DSFs) as passive absorbers to reduce the effects of wind-induced vibrations on tall buildings has been proposed by Moon in [8, 9]. A DSF is part of the building's envelope, generally designed to increase thermal efficiency and acoustic isolation [10, 11]. This system has many advantages, providing natural or mechanical ventilation (particularly during the warm seasons) as well as thermal insulation [12–14]. The DSF has been initially modelled by Moon as a single tuned mass damper (TMD) directly excited by an external sinusoidal force [8, 15], while a more realistic representation of the DSF has been proposed in further studies, with a series of TMDs vertically distributed in various configurations along the height of the building [9, 16]. The performance of DSFs as vibrating masses to control the seismic motion have been investigated by Abtahi et al. [17], who have compared the response of a building structure in three configurations, namely without DSF and with both fixed and movable DSF, showing that the latter was the most efficient configuration in reducing the structural vibrations.

Fu et al. [18, 19] have investigated five configurations of DSF modelled as TMD, comparing their performance in terms of mean-square inter-story drifts under the earthquake loads. In their studies, the two-damper and ten-damper DSF configurations resulted as the best and worst performing systems, respectively, demonstrating the importance of an appropriate design of the DSF, based on structural dynamics considerations.

Azad et al. [20, 21] have analysed the DSF to control wind-induced vibrations by modelling it as a TMD excited by a sinusoidal signal with variable frequency.

More recently, Palmeri et al. [22] have proposed a preliminary study on the coupled dynamic problem of a DSF attached to a multi-degree of freedom (MDoF) shear-type structure excited by seismic ground motions. The DSF has been modelled as a system of two independent flexible panels, connected to the main structure by elastic links. The design of the panel's stiffness and damping has been approached as a series of numerical optimisation problems, minimising the response of the main structure for various earthquake records, returning multiple optimal sets of design variables.

In this paper, an in-depth numerical analysis of this coupled dynamic problem is performed by considering multiple configurations of the DSF, using four distinct design approaches. The DSF is modelled as a set of independent panels, each one studied as a lumped mass system connected to the main structure by elastic springs at the floor levels, and the whole building-DSF system has been analysed considering a set of twenty earthquake records. The design problem aims to determine the optimal flexural stiffness of the DSF panels, the stiffness of elastic links connecting the DSF to the primary structure and the damping of the DSF. Two types of links have been considered depending on their location relative to the panel (external and internal links) which can trigger various dynamic mechanisms. These design variables have been determined by using four distinct optimisation approaches. In the first case, the objective of the optimisation problem is the minimisation of the displacement of the first storey of the primary structure; the latter is directly proportional to the maximum internal forces experienced by a shear-type frame and thus its reduction allows preserving the structural integrity of the building [23, 24]. A second set of optimisation problems, focused on serviceability limit states, has been set up to minimise the absolute acceleration of the top storey of the primary structure. For both cases, two types of fitness functions have been considered. The first one minimises the displacements (or accelerations) due to a single earthquake record. Hence, a distinct set of optimal design variables is obtained for each accelerogram. Conversely, the target of the second type of objective function is to minimise the average displacements (or accelerations) for all the twenty earthquake records, returning therefore only a single set of optimal design variables that takes into account the various seismic scenarios. Numerical results are presented for a case study, using various layouts of the DSF, modelled as a set of one, two, three or six independent panels. For each configuration, the four optimisation problems described above have been numerically solved through Particle Swarm Optimisation (PSO) algorithms. Finally, the effects of the optimal link design on the dynamic behaviour of the DSF panels is examined in detail.

DOI: 10.1002/stc

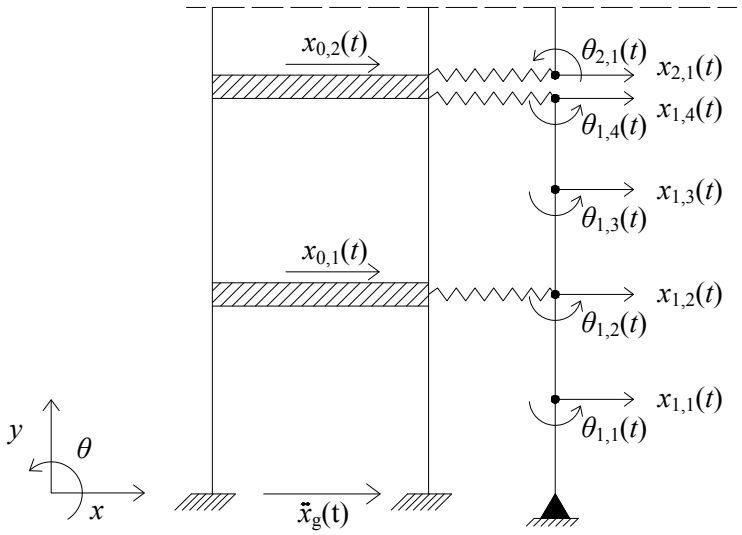

Figure 1. Sketch of the structural model.

2. PRIMARY STRUCTURE AND DSF COUPLED SYSTEM

A simplified scheme of a multi-storey structure coupled with a DSF is shown in Figure 1. Without lack of generality, the primary building is modelled as a shear-type frame having equal floor mass m_0, lateral stiffness k_0 and inter-storey height h, while the viscous damping ratio ζ_0 is assumed to be constant in all the modes of vibration. If the dynamic system is forced by a unidirectional seismic ground acceleration, $\ddot{x}_g(t)$, the equation of motion of the building can be written as:

$$\mathbf{M}_0 \cdot \ddot{\mathbf{x}}_0(t) + \mathbf{C}_0 \cdot \dot{\mathbf{x}}_0(t) + \mathbf{K}_0 \cdot \mathbf{x}_0(t) = -\mathbf{M}_0 \cdot \boldsymbol{\tau}_0 \, \ddot{x}_g(t) \,, \tag{1}$$

where: $\mathbf{x}_0(t) = \left\{ x_{0,1}(t) \quad x_{0,2}(t) \quad \cdots \quad x_{0,n_0}(t) \right\}^\top$ is the array collecting the lateral displacements of the main structure; the over-dot means time derivative; n_0 is the number of storeys in the building structure; $\boldsymbol{\tau}_0$ is the location or incidence vector; $\mathbf{M}_0$, $\mathbf{C}_0$ and $\mathbf{K}_0$ are the mass, damping and stiffness matrices, respectively, and the subscript 0 is used to identify any quantity associated with the primary structure.

In this paper, the DSF is considered as a vibration absorber with mass distributed along the height of the primary structure. Various configurations are analysed, with the DSF represented either as a single panel or as a set of N panels linked to the floors of the primary structure by elastic springs. The generic ith panel, with $i = 1, 2, \ldots, N$, is modelled as an elastic beam-like structure, discretised with two-node Euler-Bernoulli beam elements of size $h/2$ and two static degrees of freedom (DoFs) for each node, namely the lateral displacement $x_{i,j}(t)$ and rotation $\theta_{i,j}(t)$ (see Figure 1). The translational mass lumped at each node of the ith DSF panel is $m_i = \mu \, m_0/2$, proportional to half of the floor mass of the primary structure (i.e. the dimensionless coefficient μ gives the ratio of the total mass of all the DSF panels to the total mass of the main building). The effects of the rotational mass in the DSF panel is neglected, meaning that the rotational DoFs can be statically condensed [22]. Accordingly, the coupled system, i.e. primary building and DSF panels, has $n_{\text{tot}} = 3\,n_0 + (N-1)$ dynamically significant DoFs (i.e. for each storey, the horizontal translation of the storey mass and of two lamped masses in the panel, plus one DoF for each additional mass at discontinuities between panels). The equations of motion can be written in compact matrix form as:

$$\mathbf{M} \cdot \ddot{\mathbf{x}}(t) + \mathbf{C} \cdot \dot{\mathbf{x}}(t) + \mathbf{K} \cdot \mathbf{x}(t) = -\mathbf{M} \cdot \boldsymbol{\tau} \, \ddot{x}_g(t) \,. \tag{2}$$

In Eq. (2), the block vector $\mathbf{x}(t) = \left\{ \mathbf{x}_0^\top(t) \quad \mathbf{x}_1^\top(t) \quad \cdots \quad \mathbf{x}_N^\top \right\}^\top$ collects the arrays of the DoFs of all subsystems (main building and DSF panels), while $\mathbf{M}$, $\mathbf{C}$ and $\mathbf{K}$ are the corresponding mass,

Prepared using stcauth.cls
DOI: 10.1002/stc

damping and stiffness matrices, respectively, and $\boldsymbol{\tau}$ is the expanded incidence vector. The mass matrix $\mathbf{M}$ can be written in the following block form:

$$\mathbf{M} = \begin{bmatrix} \mathbf{M}_0 & \mathbf{O}_{n_0 \times n_1} & \cdots & \mathbf{O}_{n_0 \times n_N} \\ \mathbf{O}_{n_1 \times n_0} & \mathbf{M}_1 & \cdots & \mathbf{O}_{n_1 \times n_N} \\ \vdots & \vdots & \ddots & \vdots \\ \mathbf{O}_{n_N \times n_0} & \mathbf{O}_{n_N \times n_1} & \cdots & \mathbf{M}_N \end{bmatrix}, \tag{3}$$

where the matrices $\mathbf{M}_i = m_i \, \mathbf{I}_{n_i}$, with $i = 0, 1, \ldots, N$, are the diagonal mass matrices of the individual components, while the symbol $\mathbf{O}_{r \times s}$ stands for the zero matrix with r rows and s columns and $\mathbf{I}_s$ is the identity matrix of size s. Analogously, the stiffness matrix can be written in the following block form:

$$\mathbf{K} = \begin{bmatrix} \mathbf{K}_0 & \mathbf{K}_{01} & \ldots & \mathbf{K}_{0N} \\ \mathbf{K}_{01}^{\top} & \tilde{\mathbf{K}}_1 & \ldots & \mathbf{O}_{n_1 \times n_N} \\ \vdots & \vdots & \ddots & \vdots \\ \mathbf{K}_{0n_p}^{\top} & \mathbf{O}_{n_N \times n_1} & \ldots & \tilde{\mathbf{K}}_N \end{bmatrix}, \tag{4}$$

where: $\mathbf{K}_0$ is the stiffness matrix of the primary structure; $\tilde{\mathbf{K}}_i$, with $i = 1, \ldots, N$, is the statically-condensed stiffness matrix of the ith DSF panel, while the block $\mathbf{K}_{0i}$ contains the stiffness coefficients of the elastic links connecting the ith DSF panel to the main building.

In this paper, the panel flexural stiffness and the link stiffness have been assumed as proportional to the storey stiffness k_0. In particular, the panel stiffness will be indicated as νk_0, and the link ones αk_0 and βk_0 depending on their relative position in the DSF panels (external and internal springs will be named α-type and β-type springs, respectively).

The damping matrix $\mathbf{C}$ of the coupled building-DSF system has been obtained by assuming that each subsystem, individually considered, is classically damped. The following expression has been used [25]:

$$\mathbf{C} = \boldsymbol{\Gamma}^{-\top} \cdot \boldsymbol{\Xi} \cdot \boldsymbol{\Gamma}^{-1} \tag{5}$$

in which $\boldsymbol{\Gamma}$ is a convenient transformation matrix and $\boldsymbol{\Xi}$ collects the modal damping coefficients :

$$\boldsymbol{\Gamma} = \begin{bmatrix} \boldsymbol{\Phi}_0 & \mathbf{O}_{n_0 \times n_1} & \cdots & \mathbf{O}_{n_0 \times n_N} \\ \boldsymbol{\Psi}_1 & \boldsymbol{\Phi}_1 & \cdots & \mathbf{O}_{n_1 \times n_N} \\ \vdots & \vdots & \ddots & \vdots \\ \boldsymbol{\Psi}_N & \mathbf{O}_{n_N \times n_1} & \cdots & \boldsymbol{\Phi}_N \end{bmatrix}; \quad \boldsymbol{\Xi} = \begin{bmatrix} 2\,\zeta_0\,\boldsymbol{\Omega}_0 & \mathbf{O}_{n_0 \times n_1} & \cdots & \mathbf{O}_{n_0 \times n_N} \\ \mathbf{O}_{n_1 \times n_0} & 2\,\zeta_{\mathrm{P}}\,\boldsymbol{\Omega}_1 & \cdots & \mathbf{O}_{n_1 \times n_N} \\ \vdots & \vdots & \ddots & \vdots \\ \mathbf{O}_{n_N \times n_0} & \mathbf{O}_{n_N \times n_1} & \cdots & 2\,\zeta_{\mathrm{P}}\,\boldsymbol{\Omega}_N \end{bmatrix}, \tag{6}$$

in which: ζ_{P} is the viscous damping matrix of the DSF panels, assumed to be the same for all the N panels; the square matrices $\boldsymbol{\Omega}_i = \mathrm{diag}\,\{\omega_{i,1}, \cdots, \omega_{i,n_i}\}$ and $\boldsymbol{\Phi}_i = [\boldsymbol{\phi}_{i,1}, \cdots, \boldsymbol{\phi}_{i,n_i}]$, of size n_i, with $0 \leq i \leq N$, are the spectral matrix and the modal matrix of the ith subsystem, respectively, and can be calculated as solution of the real-valued eigenproblem:

$$\mathbf{M}_i \cdot \boldsymbol{\Phi}_i \cdot \boldsymbol{\Omega}_i^2 = \mathbf{K}_i \cdot \boldsymbol{\Phi}_i \,, \tag{7}$$

with the normalisation condition $\boldsymbol{\Phi}_i^{\top} \cdot \mathbf{M}_i \cdot \boldsymbol{\Phi}_i = \mathbf{I}_{n_i}$, while, for $1 \leq i \leq N$, the modal influence matrix $\boldsymbol{\Psi}_i$ can be evaluated as:

$$\boldsymbol{\Psi}_i = -\tilde{\mathbf{K}}_i^{-1} \cdot \mathbf{K}_{0i}^{\top} \cdot \boldsymbol{\Phi}_0 \,. \tag{8}$$

3. DSF OPTIMISATION CRITERIA

The optimal design of DSFs as vibration absorbers is not straightforward as, for a given primary building structure and a given mass ratio μ, the dynamic performance depends on the chosen

DOI: 10.1002/stc

configuration (i.e. number of DSF panels, N), the structural parameters of panels and links (ν, α, β and ζ_{P}) as well as the objective of the optimisation problem. In this paper, various strategies have been considered, varying the optimisation criteria and the DSF configurations; namely, four optimisation approaches have been used to compare various design solutions matching different optimisation criteria.

All the objective functions have been defined in terms of the normalised standard deviation $\sigma(y)$ of a selected dynamic response $y(t)$ of the main structure to one or more earthquake records, calculated in the observation time window $t \in [t_{\mathrm{a}}, t_{\mathrm{b}}]$, whose extremes depend on the so-called Husid function $\mathcal{H}(t)$, given by [26]:

$$\mathcal{H}(t) = \frac{\int_0^t \ddot{x}_{\mathrm{g}}^2(t)\,\mathrm{d}t}{\int_0^{t_{\mathrm{eq}}} \ddot{x}_{\mathrm{g}}^2(t)\,\mathrm{d}t}\,, \tag{9}$$

where t_{eq} is the duration of the earthquake record, and thus $0 \leq \mathcal{H}(t) \leq 1$. Assuming that the strong motion phase of a given seismic record is bounded by the time instants t_{05} and t_{95} at which $\mathcal{H}(t)$ takes the values 0.05 and 0.95, respectively, the extremes t_{a} and t_{b} have been computed for each accelerogram as $t_{\mathrm{a}} = t_{05}$ and $t_{\mathrm{b}} = t_{95} + t_{\mathrm{tr}}$, in which the transient time t_{tr} satisfies the condition:

$$\mathrm{e}^{-\zeta_0\,\omega_{0,1}\,t_{\mathrm{tr}}} = 0.05\,; \tag{10}$$

that is, t_{tr} is the time required for the seismic response of the main structure in its fundamental mode of vibration to reduce to 5% of its amplitude at the end of the the strong motion phase, $\omega_{0,1} = 2\pi/T_{0,1}$ being the first modal circular frequency of the primary system and $T_{0,1}$ the corresponding period of vibration. It follows that, for $\zeta_0 = 0.02$, $t_{\mathrm{tr}} \approx 24\,T_{0,1}$.

3.1. Displacement-based vs acceleration-based optimisation

The structural integrity of the primary system is dependent on the amount of internal forces acting on its members. In particular, assuming a shear-type frame model, the maximum internal forces are proportional to the displacements of its first storey, i.e. the relevant EDP (engineering demand parameter) is $y(t) = x_{0,i}(t)$. Hence, the first proposed optimisation approach is based on the following objective functions:

$$J_{1,ER} = \frac{\sigma(x_{0,1,ER})^{\mathrm{C}}}{\sigma(x_{0,1,ER})^{\mathrm{U}}}\,, \tag{11}$$

where $\sigma(x_{0,1,ER})^{\mathrm{C}}$ and $\sigma(x_{0,1,ER})^{\mathrm{U}}$ are the standard deviations of the displacements of the first storey of the primary structure due to the eth earthquake record, with and without the attached DSF, respectively (i.e. controlled and uncontrolled structure).

Since the function $J_{1,ER}$ is calculated for each earthquake, a different set of design variables is obtained for each accelerogram. While this approach guarantees the best DSF performance for a given record, nothing can be said on the performance of the DSF for a different excitation. Nevertheless, this approach can be used to observe the variations of the optimal design parameters when the external excitation changes.

The second objective function has been defined as the average of $J_{1,ER}$ for a number n_{ER} of recorded accelerograms. Since the coupled building-DSF structure is linear, then:

$$J_2 = \frac{1}{n_{\mathrm{ER}}} \sum_{e=1}^{n_{\mathrm{ER}}} J_{1,ER}\,. \tag{12}$$

This corresponds to minimise the sum of the standard deviations of the structural response to the selected earthquakes, normalising them so that the standard deviation of the uncontrolled response is constant.

Two additional optimisation approaches have also been investigated to take into account the serviceability of the main structure. In this case, the absolute acceleration of the top storey of the

Prepared using stcauth.cls
DOI: 10.1002/stc

primary system, $y(t) = \ddot{x}^{(\mathrm{a})}_{0,n_0}(t)$, has been considered as the EDP to be controlled and, analogously to the displacement-based optimisation problem, the following objective functions have been defined:

$$J_{3,ER} = \frac{\sigma(\ddot{x}^{(\mathrm{a})}_{0,n_0,ER})^{\mathrm{C}}}{\sigma(\ddot{x}^{(\mathrm{a})}_{0,n_0,ER})^{\mathrm{U}}}\,; \tag{13}$$

$$J_4 = \frac{1}{n_{\mathrm{ER}}} \sum_{e=1}^{n_{\mathrm{ER}}} J_{3,ER}\,. \tag{14}$$

4. NUMERICAL APPLICATIONS

In this section, the design optimisation for the six-storey building model depicted in Figure 2 is presented ($n_0 = 6$). The main structure has fundamental period of vibration $T_{0,1} = 2\pi/\omega_{0,1} = 0.582s$ and viscous damping coefficient $\zeta_0 = 0.02$. Effects of soil-structure interaction (e.g. interaction forces between foundations and underlying soil due to their relative translations and rotations) have been neglected in the analysis. Readers are referred to [27] for detail on the relevance of this phenomenon on the design of passive control devices. The DSF mass has been fixed considering a mass ratio $\mu = 0.1$. Four different configurations have been studied to analyse all possible combinations of panels covering whole numbers of storeys of the primary structure, i.e.:

(a) a single panel ($N = 1$) hinged to the ground and connected to the primary structure by one α-type and five β-type springs;

(b) two panels ($N = 2$), the lowest one hinged to the ground (this is the same configuration analysed in Ref. [22]);

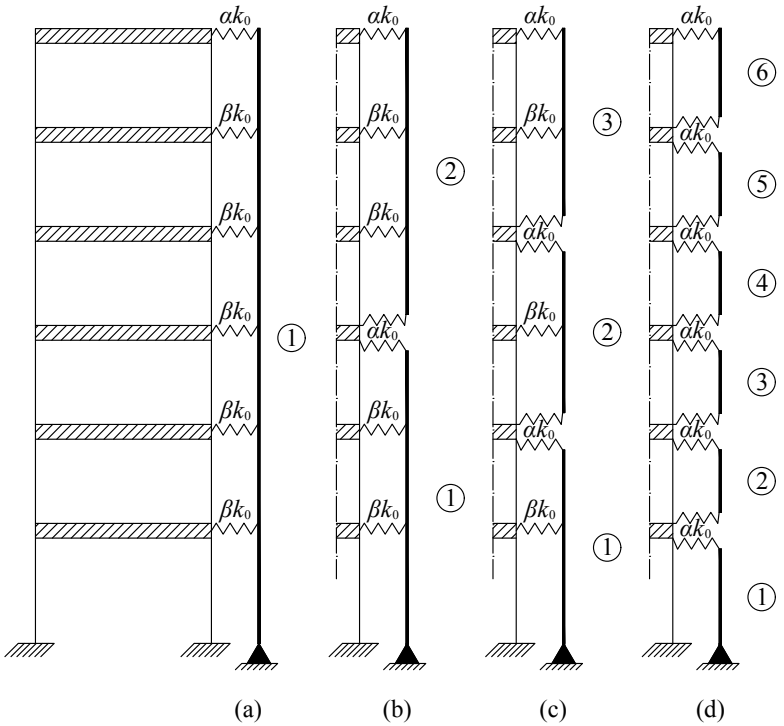

Figure 2. Coupled dynamic system with different DSF configurations: 1 Panel (a), 2 Panels (b), 3 Panels (c) and 6 Panels (d).

DOI: 10.1002/stc

Table I. Set of earthquake records used for the numerical optimisation.

No.	Epicentre	Date	Peak acc. [g]	Duration [s]
1	Parkfield, California	27/06/1966	0.434	44.04
2	Pacomia Dam, California	09/02/1971	1.075	41.74
3	Helena, Montana	31/10/1935	0.147	50.96
4	Wrightwood, California	12/09/1970	0.198	16.72
5	Lake Hughes, California	09/02/1971	0.146	37.02
6	Iverson, Canada	23/12/1985	1.102	20.34
7	Yoneyama Bridge, Japan	26/02/1971	0.151	17.06
8	El Centro, California	18/05/1940	0.348	53.74
9	T. Lincon School Tunnel, California	21/07/1952	0.179	54.40
10	Monte Negro, Yugoslavia	19/04/1979	0.171	40.40
11	La Villita, Guerrero Array, Mexico	19/09/1985	0.123	64.02
12	El Centro, California	30/12/1934	0.160	44.04
13	Sturno, Italy	11/11/1980	0.358	39.34
14	Duzce, Turkey	12/11/1999	0.535	25.89
15	Takatori, Japan	16/01/1995	0.611	40.96
16	Tabas, Iran	16/09/1978	0.836	32.84
17	Erizikan, Turkey	13/03/1992	0.515	21.31
18	Kalamata, Greece	13/09/1986	0.248	12.19
19	Loma Prieta, California	18/10/1989	0.966	25.00
20	Tolomezzo, Italy	06/05/1980	0.351	36.35

(c) three panels ($N = 3$), the lowest one hinged to the ground;

(d) six panels ($N = 4$), one per storey, the lowest one hinged to the ground.

For each of the four configurations, the displacement-based and acceleration-based objective functions J_k proposed in Section 3.1 have been minimised using the PSO algorithm [28–30], considering the twenty earthquake records reported in Table I; this corresponds to a total number of $4 \times 2 \times (20 + 1) = 168$ optimisation problems. Each of them can be formally written as:

$$\text{Given:} \quad m_0\,,\, k_0\,,\, \zeta_0\,,\, \ddot{x}_{\mathrm{g}}(t)\,,\, \text{geometry}\,; \tag{15a}$$

$$\text{Find:} \quad \nu\,,\, \alpha\,,\, \beta\,,\, \zeta_{\mathrm{P}}\,; \tag{15b}$$

$$\text{To minimise:} \quad J_k\,; \tag{15c}$$

$$\text{Such that:} \quad \begin{cases} \nu_{\min} \leq \nu \leq \nu_{\max}\,; \\ \alpha_{\min} \leq \alpha \leq \alpha_{\max}\,; \\ \beta_{\min} \leq \beta \leq \beta_{\max}\,; \\ \zeta_{\min} \leq \zeta_{\mathrm{P}} \leq \zeta_{\max}\,, \end{cases} \tag{15d}$$

DOI: 10.1002/stc

where the following values have been chosen for the numerical constraints on the design variables in order to get physically consistent results:

$$\begin{cases} \nu_{\text{min}} = \zeta_{\text{min}} = 10^{-4}\,; \\ \alpha_{\text{min}} = \beta_{\text{min}} = 10^{-6}\,; \\ \nu_{\text{max}} = 0.5\,; \\ \alpha_{\text{max}} = \beta_{\text{max}} = 0.1\,; \\ \zeta_{\text{max}} = 0.2\,. \end{cases} \tag{16}$$

4.1. Displacement-based optimisation

This methodology returned large variations of the design variables in the search space, making impossible to identify an efficient design valid for all possible scenarios. Tables II and III provide the results for two selected cases, namely $\text{DBO}_{5,PL}$ and $\text{DBO}_{12,PL}$ (bold fonts indicate boundary values). The most efficient DSF layout is configuration (c) for the first case ($ER = 5$); configuration (a) for the second case ($ER = 12$). While the values of the objective functions $J_{1,ER}$ are comparable in these two circumstances (i.e. the effectiveness of the DSF is similar), still the optimal design variables, for all configurations, are very different. In particular, the stiffness of the elastic links shows very drastic changes for different earthquakes records. It has also been observed that the effectiveness of a DSF optimised for a given earthquake record is very likely to be significantly less for a different seismic event. To take into account the overall effects off the selected earthquakes, an "average displacement-based optimisation" (ADBO_{PL}) has been performed minimising the objective function J_2 for each of the four proposed configurations. Numerical results are reported in Table IV. Again, it can be observed that the four configurations have similar effectiveness (i.e. they return similar values for the function J_2), with configuration (a) performing slightly better than the others. The design variables significantly differ from one configuration to the other, and only the damping coefficient ζ_{P} varies in a limited range, with $\zeta_{\text{P}} \in [0.10\,, 0.16]$.

In Figure 3 the modulus of the transfer functions $H(\omega)$ of the uncontrolled (UNC) primary building (black dashed lines) is compared with those of all the different displacement-based optimal designs of the DSF ($\text{DBO}_{ER,PL}$ with grey thin lines and ADBO_{PL} with red dashed line); the envelope obtained for the twenty earthquake records (ENV) is also reported (black solid lines).

Table II. Design values obtained by $\text{DBO}_{5,PL}$.

Config.	ζ_P [%]	ν	α	β	$J_{1,5}$ [%]
(a)	6.12	3.12×10^{-1}	4.11×10^{-3}	3.74×10^{-3}	38.06
(b)	4.57	5.30×10^{-2}	3.89×10^{-2}	$\mathbf{10^{-6}}$	34.72
(c)	5.12	1.02×10^{-2}	2.55×10^{-2}	$\mathbf{10^{-6}}$	33.09
(d)	7.64	2.71×10^{-3}	2.59×10^{-3}	-	36.26

Table III. Design values obtained by $\text{DBO}_{12,PL}$.

Config.	ζ_P [%]	ν	α	β	$J_{1,12}$ [%]
(a)	6.53	4.80×10^{-1}	4.34×10^{-3}	4.28×10^{-3}	36.61
(b)	8.27	1.67×10^{-1}	$\mathbf{10^{-6}}$	7.90×10^{-3}	37.14
(c)	8.82	3.71×10^{-2}	$\mathbf{10^{-6}}$	1.09×10^{-2}	37.11
(d)	9.28	5×10^{-1}	2.48×10^{-3}	-	37.66

DOI: 10.1002/stc

Table IV. Design values obtained by ADBO_{PL}.

Config.	ζ_P [%]	ν	α	β	J_2 [%]
(a)	10.5	5.89×10^{-2}	5.13×10^{-3}	3.99×10^{-3}	52.86
(b)	14.0	1.35×10^{-1}	$\mathbf{10^{-6}}$	7.64×10^{-3}	53.61
(c)	11.4	3.18×10^{-2}	2.99×10^{-6}	1.06×10^{-2}	53.62
(d)	15.5	$\mathbf{0.5}$	2.49×10^{-3}	-	52.92

In all cases, the major effect of the DSF is to reduce the magnitude of the peak of the transfer function in the first mode of vibration. Increasing the number of panels (i.e. moving from configuration (a) towards configuration (d)) tends to increase the effects on the higher modes. In particular, the maximum effect on higher modes seems to be consistently obtained for configuration (c). Furthermore, as expected, the transfer function corresponding to the case ADBO_{PL} shows an intermediate behaviour with respect to the twenty $\text{DBO}_{ER,PL}$ for the same PLth configuration. A comparison of the transfer functions for the different ADBOs is shown in Figure 4, where it can be noted that varying the DSF configuration only marginally affects the overall dynamic behaviour of the DSF-controlled building. Finally, Figure 5 shows the overall response of the system for configuration (b), with two DSF panels, in terms of the objective function $J_{1,ER}$ for all the selected earthquakes. For the ERth seismic excitation, the diagram shows the range of variation of the function $J_{1,ER}$ using all considered $\text{DBO}_{ER,\text{b}}$ (grey lines). Values for two selected design options, namely $\text{DBO}_{5,\text{b}}$ and $\text{DBO}_{12,\text{b}}$, are highlighted together with the average design ADBO_{b}. Obviously, these design options give the maximum response reduction (minimum value of $J_{1,ER}$) for the corresponding earthquake (e.g., $\text{DBO}_{5,\text{b}}$ for record $ER = 5$), while they are less effective, or almost ineffective, for the other cases. On the contrary, the case ADBO_{b} shows high effectiveness for all the considered earthquake records (although it is never the best design option for any given accelerogram).

DOI: 10.1002/stc

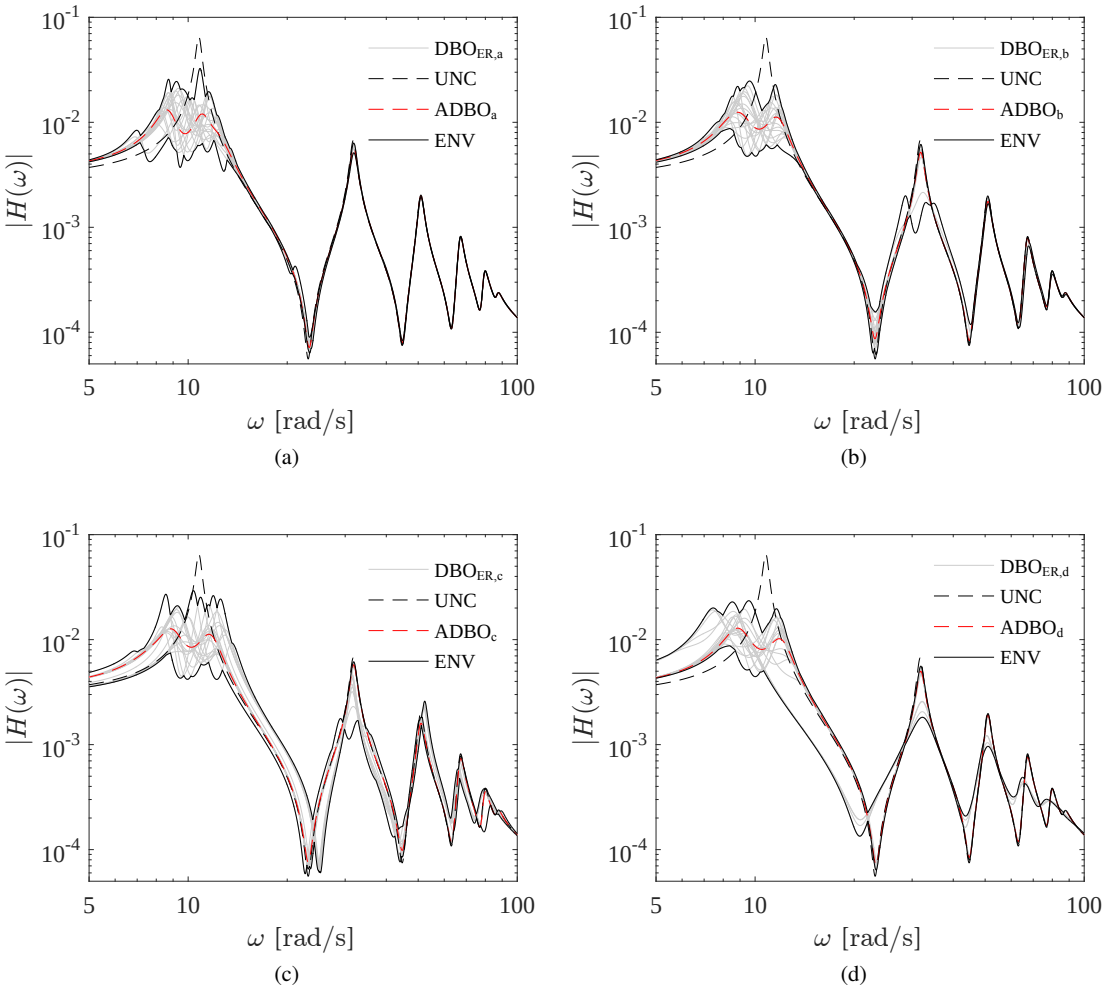

Figure 3. Transfer functions $H(\omega)$ for DSF configurations (a) to (d) considering: $\text{DBO}_{ER,PL}$ values (gray lines) and their envelope (black lines); uncontrolled case (black dashed line); ADBO_{PL} values (red dashed line).

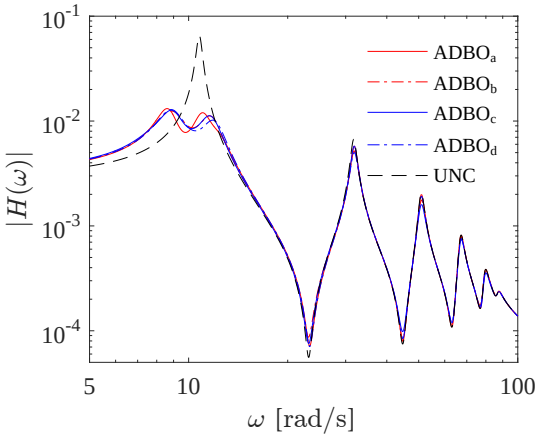

Figure 4. Transfer functions for ADBO_{PL} values.

DOI: 10.1002/stc

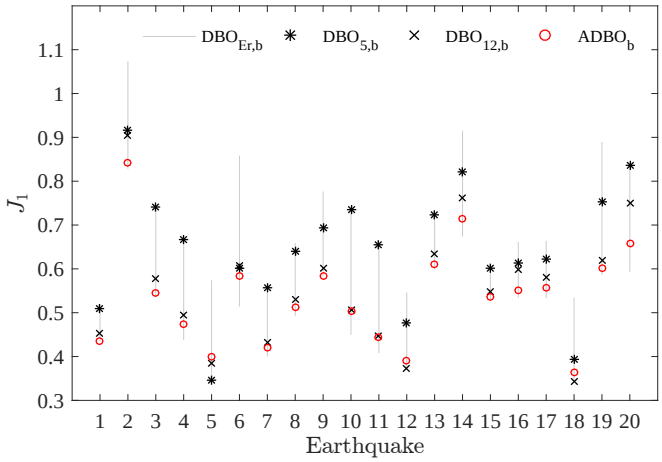

Figure 5. $J_{1,i}$ values for configuration (b), obtained for: $\text{DBO}_{ER,\text{b}}$ values (gray lines), $\text{DBO}_{5,\text{b}}$ (black asterisk), $DBO_{12,\text{b}}$ (black cross), ADBO_{b} (red cycle) values.

4.2. Acceleration-based optimisation

A similar methodology has been applied for the objective functions $J_{3,ER}$ and J_4, defined in terms of absolute accelerations of the top storey of the main structure. At first, 80 sets of optimal design variables have been compared by minimising the function $J_{3,ER}$ for the twenty earthquake records and the four DSF layouts. Even if a single set of optimal values for the design variables could not be obtained by the "acceleration-based optimisation" ($\text{ABO}_{ER,PL}$), results suggest that configuration (d) has the best performance among the proposed ones. Similarly to the previous subsection, Table V and VI report numerical results for $\text{ABO}_{5,PL}$ and $\text{ABO}_{12,PL}$. On the other hand, results from the "average acceleration-based optimisation" (AABO_{a-d}), that minimises the objective function J_4, are shown in Table VII. Again, configuration (d) returns the minimum value for J_4. The only design variable that does not have significant variations is ζ_{P}. The dynamic effects of all the discussed DSF designs are summarised in Figure 6, showing all the corresponding transfer functions $H(\omega)$, and Figure 7 where only the AABO_{PL} are compared. Among the latter, configuration (d) has a unique dynamic behaviour, affecting all the natural modes of the main structure, which explains its improved performance.

Finally, Figure 8 shows values of $J_{3,ER}$ for configuration (b), for all the earthquakes. The range of variation of $J_{3,ER}$ is reported with grey lines. The values for $\text{ABO}_{5,\text{b}}$ and $\text{ABO}_{12,\text{b}}$ are highlighted and compared with the AABO_{b}. As expected, analogously to the displacement-based optimisation, the average design (AABO_{b}) is highly effective in all cases, while the $\text{ABO}_{ER,\text{b}}$ only acts properly for the ERth earthquake.

Table V. Design values obtained by $\text{ABO}_{5,PL}$.

Config.	ζ_P [%]	ν	α	β	$J_{3,5}$ [%]
(a)	4.01	**0.5**	$\mathbf{10^{-6}}$	1.88×10^{-3}	59.47
(b)	3.68	5.81×10^{-2}	3.60×10^{-2}	$\mathbf{10^{-6}}$	53.05
(c)	3.36	1.11×10^{-2}	2.47×10^{-2}	$\mathbf{10^{-6}}$	53.08
(d)	**20**	**0.5**	9.66×10^{-2}	-	49.72

DOI: 10.1002/stc

Table VI. Design values obtained by $\text{ABO}_{12,PL}$.

Config.	ζ_P [%]	ν	α	β	$J_{3,12}$ [%]
(a)	7.46	3.75×10^{-2}	4.49×10^{-3}	4.48×10^{-3}	47.44
(b)	7.55	1.72×10^{-1}	$\mathbf{10^{-6}}$	8.89×10^{-3}	46.65
(c)	9.26	3.37×10^{-2}	1.10×10^{-4}	1.22×10^{-2}	47.17
(d)	**20**	**0.5**	**0.1**	-	38.36

Table VII. Design values obtained by AABO_{PL}.

Config.	ζ_P [%]	ν	α	β	J_4 [%]
(a)	13.2	5.5×10^{-4}	1.15×10^{-2}	6.72×10^{-3}	68.44
(b)	12.0	6.49×10^{-2}	3.05×10^{-2}	$\mathbf{10^{-6}}$	68.29
(c)	15.8	2.23×10^{-2}	4.08×10^{-5}	1.31×10^{-2}	69.25
(d)	**20**	**0.5**	**0.1**	-	65.09

DOI: 10.1002/stc

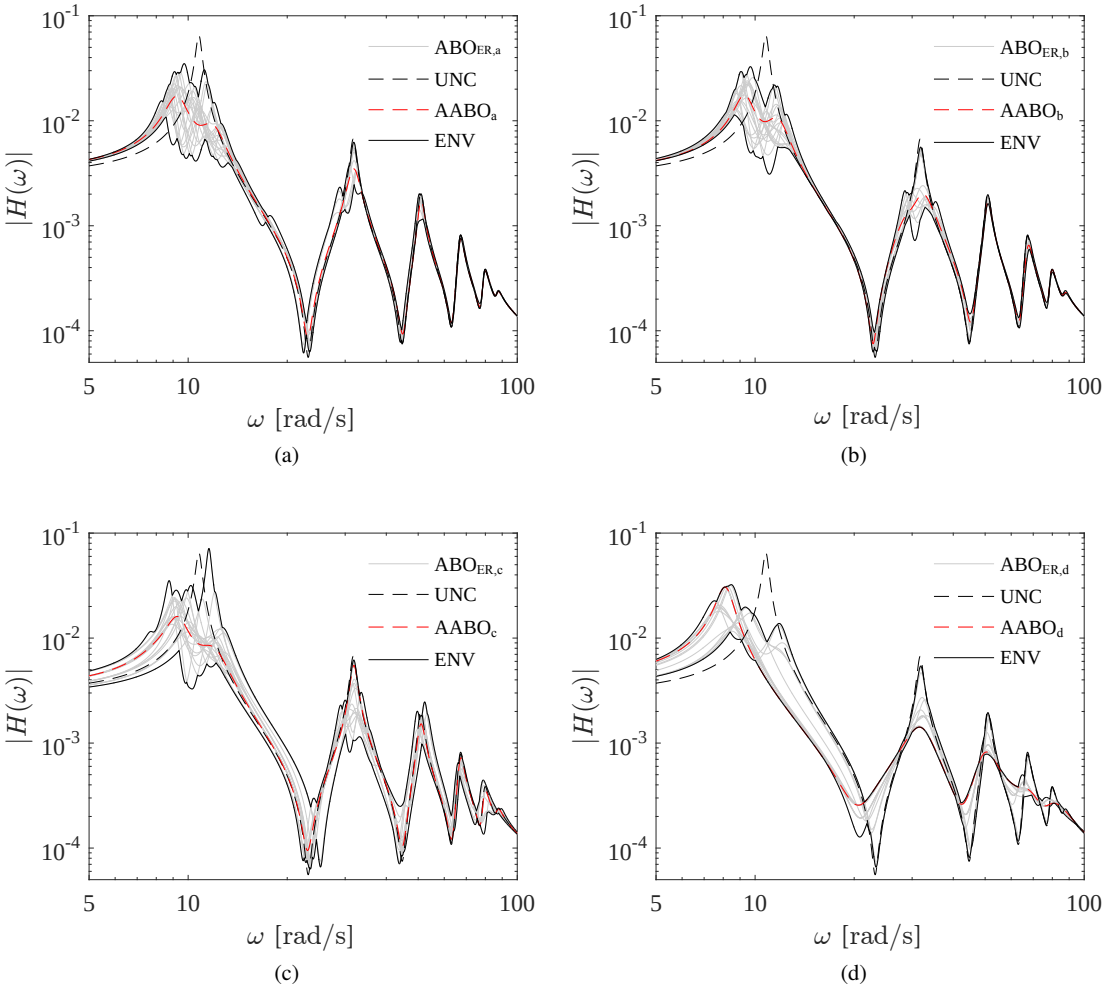

Figure 6. Transfer functions $H(\omega)$ for DSF configurations (a) to (d) considering: $\text{ABO}_{ER,PL}$ values (gray lines) and their envelope (black lines); uncontrolled case (black dashed line), AABO_f values (red dashed line).

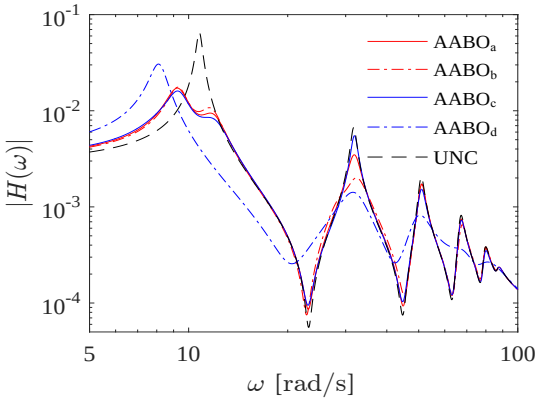

Figure 7. Transfer functions for $AABO_{a-d}$ values.

DOI: 10.1002/stc

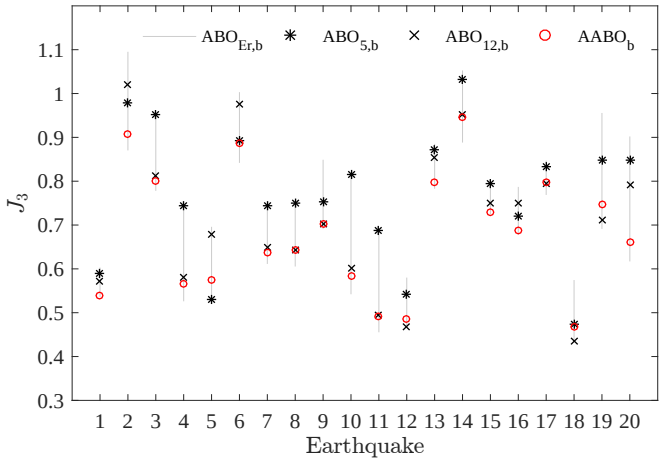

Figure 8. $J_{3,e}$ values for configuration (b), obtained for: $\mathrm{ABO}_{ER,\mathrm{b}}$ values (gray lines), $\mathrm{ABO}_{5,\mathrm{b}}$ (black asterisk), $\mathrm{ABO}_{12,\mathrm{b}}$ (black cross), $\mathrm{AABO}_{\mathrm{b}}$ (red cycle) values.

5. EFFECTS OF LINK DESIGN ON DSF PERFORMANCE

The results of the numerical investigations reported in the previous section have revealed great variations in the optimal design values of the DSF, depending on the chosen configuration and optimisation criteria. However, specific trends were observed in the values taken by the α and β coefficients, which represent the normalised stiffness of the elastic links connecting the main building and the DSF panels.

With the aim of understanding how the link design affects the dynamic behaviour of the coupled building-DSF system, a further numerical study has been performed for assigned values of the panel stiffness and damping (i.e. fixed values of ν and ζ_{P}), assumed as their average $\mathrm{DBO}_{ER,PL}$ values for each configuration; then, $J_{1,ER}$ and $J_{3,ER}$ have been plotted, in a 3-dimensional space, as functions of α and β for the configurations (a) to (c) (there are no β-type springs in configuration (d)).

Figure 9 shows, for example, the functions $J_{1,5}$ and $J_{3,5}$ computed for configuration (a), (b) and (c), respectively, versus $\log(\alpha)$ and $\log(\beta)$. A region of maximum effectiveness of the DSF can be clearly identified in all three cases (blue area), where the maximum reduction of the displacements and accelerations of the main structure occurs. The same behaviour can be observed for all the seismic records and DSF configurations which have been tested.

Figure 10 depicts the projection on the $\alpha - \beta$ plane of the loci of points of maximum effectiveness for all the analysed earthquakes. It is possible to identify three distinct subregions, namely:

- I: a region (horizontal lines) where $\beta \gg \alpha$ (up to four orders of magnitude), i.e. the external springs stiffness is negligible compared to the internal ones, meaning that most of the vibrations in the DSF panels will happen in their top and bottom parts;
- II: a curved region where α and β have similar order of magnitude, therefore both internal and external springs have comparable stiffness, so that all the springs will tend to contribute to the vibrations in the DSF panels;
- III: a region with $\alpha \gg \beta$ (vertical lines), indicating that the internal springs have negligible stiffness compared to the external ones and therefore most of the vibration will occur in the central part of the DSF panels.

DOI: 10.1002/stc

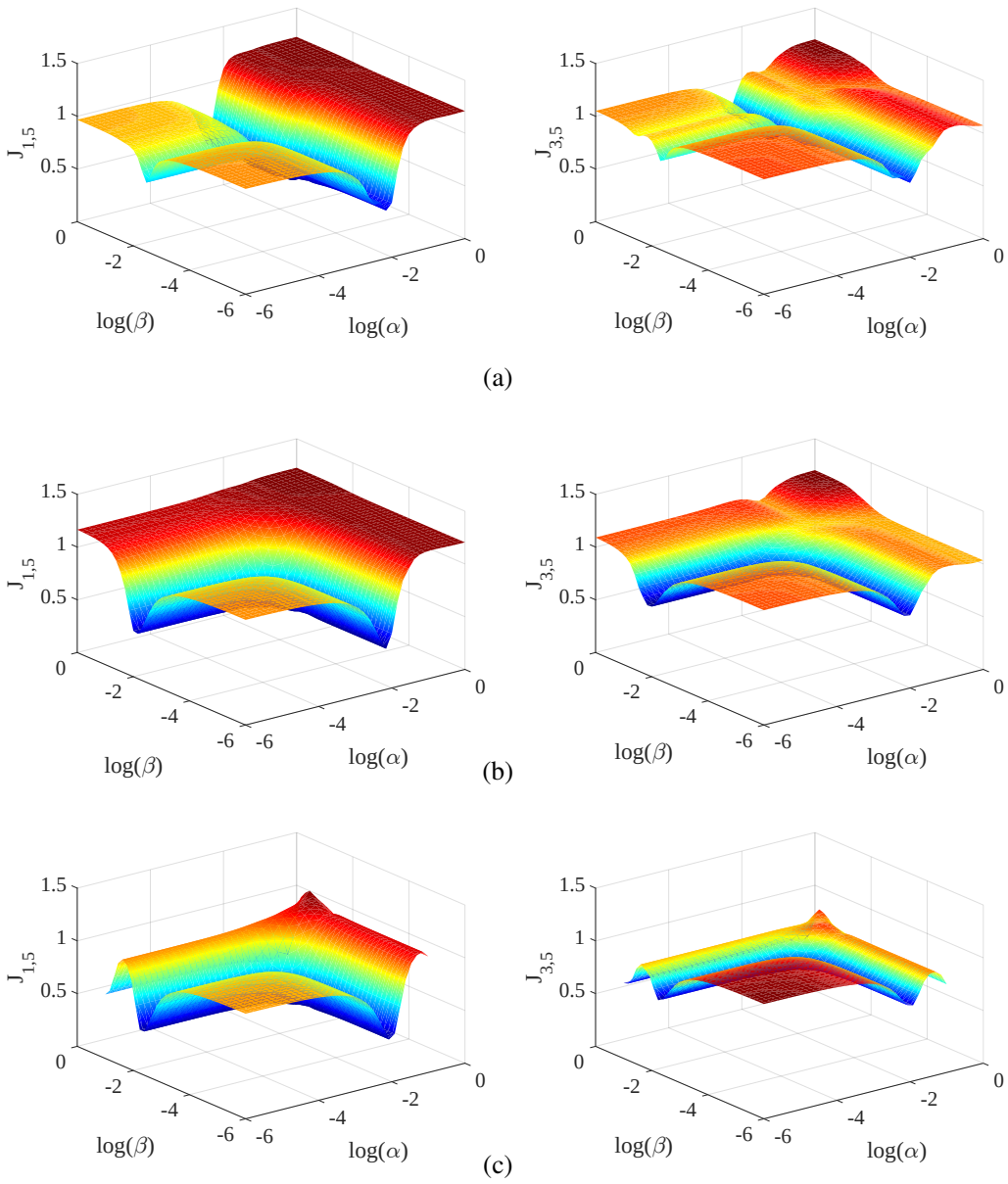

Figure 9. Objective functions $J_{1,5}$ and $J_{3,5}$ for configurations (a) to (c), considering average panel stiffness of ν and ζ_P.

DOI: 10.1002/stc

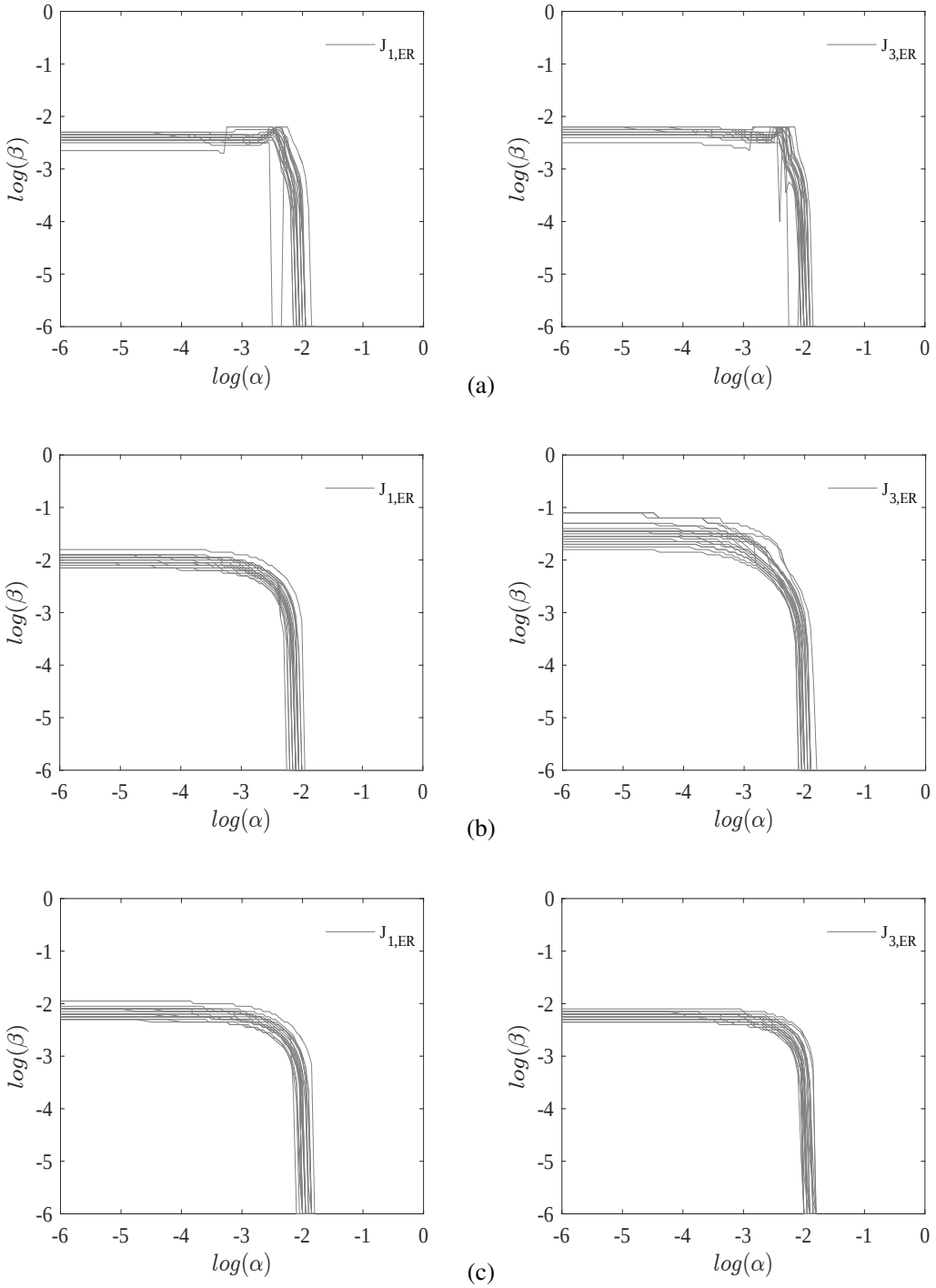

Figure 10. Projection of all $J_{1,i}$ and $J_{3,i}$ minima for DSF configurations (a) to (c).

DOI: 10.1002/stc

Figure 11 shows the modal shapes associated with the peaks of the transfer functions of the relative displacements of the panels with respect to the primary structure. These modal shapes are depicted for different layouts of the DSF ((a), (b), (c)) and for three different sets of link stiffness representative of the regions I, II, and III, respectively. In general, these peaks correspond to the first mode of the panels, assumed as fixed at the point of attachment with the primary structure. However, the peaks shift on the second mode when the link stiffness belongs to region III for the layout (a), and to region I for the top and middle panels of layout (c).

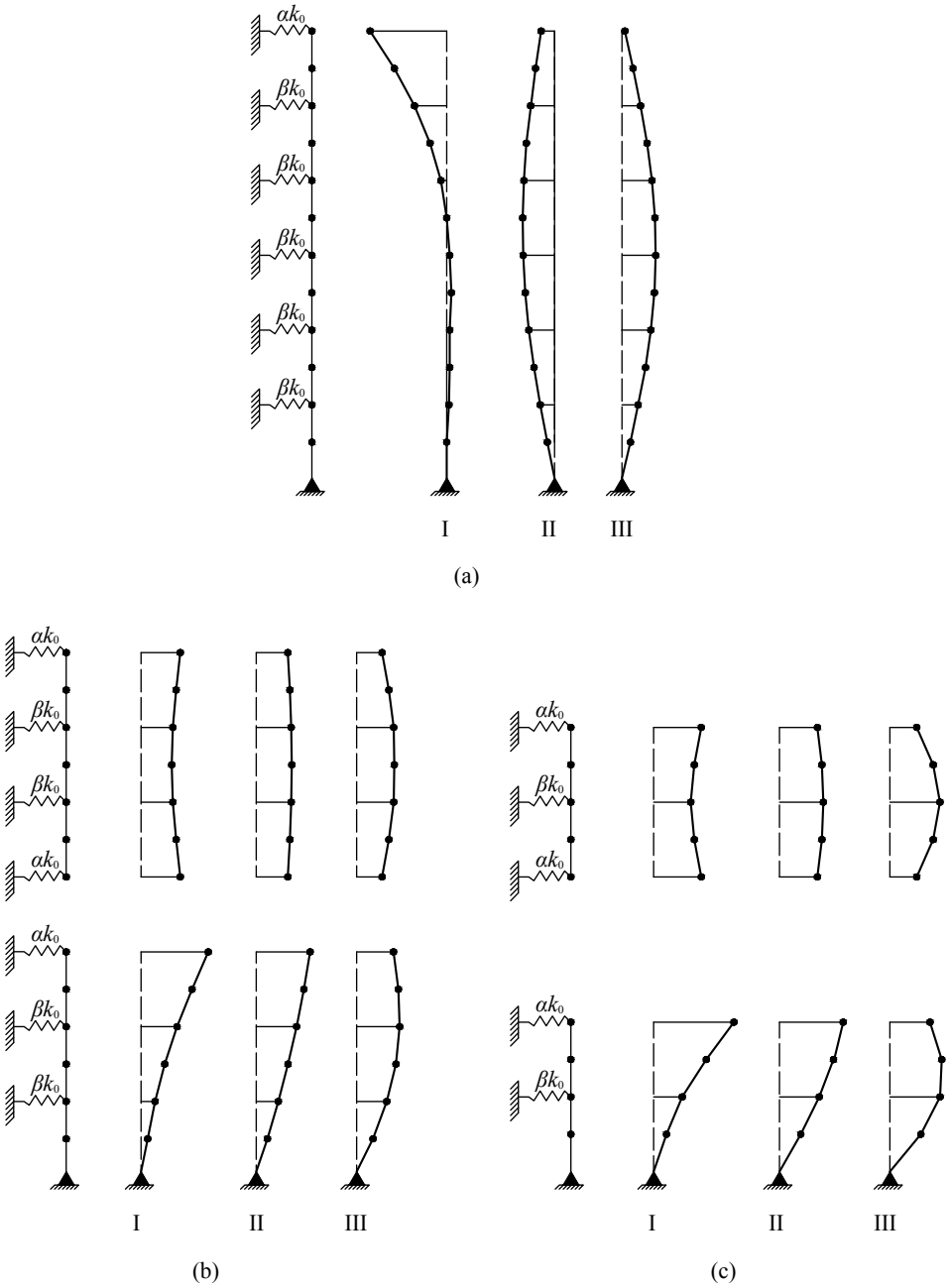

Figure 11. Modal shapes of the DSF panels in configuration (a), (b) and (c) for: I ($\alpha = 10^{-5.5}$, $\beta = 10^{-2}$), II ($\alpha = \beta = 10^{-3.5}$), III ($\alpha = 10^{-2}$ and $\beta = 10^{-5.5}$).

DOI: 10.1002/stc

6. CONCLUSIONS

In this paper, the use of double skin façades (DSFs) as distributed vibration absorbers for passive control of structures subjected to seismic excitation has been investigated. Four different configurations of the DSF have been studied, made of independent panels connected to the main structure by elastic links with viscous damping. The design of the DSF has been approached as an optimisation problem, minimising the standard deviation of either the inter-storey drifts or the absolute accelerations in the main structure. In both cases, the optimisation problem has been studied for several recorded earthquakes, comparing the various resulting design options at first, and then using an average objective function that simultaneously takes into account multiple records at once.

The numerical analysis of a case study shows that the optimisation of the DSF based on a single earthquake record does not provide robust results, while the second approach, that considers multiple events, allows identifying a design of the panel that, although non-optimal for each single case, still is highly effective for any seismic excitation. The most significant impact of the DSF is on the first mode of the main structure; however, configurations with multiple panels (in particular, spanning two or three storeys) can also have an effect on the higher modes.

Finally, an in-depth analysis of the link "optimal" design has been conducted. It has been observed that an effective design implies either to consider all springs with equal stiffness (with a consequent translational motion of the panel itself), or to have external (or internal) springs significantly stiffer than the remaining ones, which would then result in a concentration of the vibration.

The application of the proposed design approach entails the following steps:

- Based on the requirements of relevant building codes and existing hazard maps, a set of earthquake records should be selected for the numerical analyses. In this work, 20 earthquake records have been considered, however the amount of available historical records could be different for each considered case, depending on existent data bases.
- An appropriate objective function has to be defined, depending on the considered limit state. Although results reported in this paper are determined considering the variance of displacements and accelerations of selected storeys of the building, a different metric could be selected (e.g. maximum relative displacements). Nevertheless, a single metric for all considered earthquake records should be used to maximise the effectiveness of the damping system under different excitations.
- The minimisation of the objective function can be achieved using any adequate optimisation algorithm. The authors have considered both Genetic Algorithms (GAs) and Particle Swarm Optimisation (PSO) in the past (the latter resulting slightly more efficient than the former). However, other optimisation techniques are available in literature and can be used instead.
- DSF layouts can be selected based on physical and technological constraints. Based on the outcomes of the case-study structure analysed in this paper, configurations with multiple panels seem to be more effective and able to resonate with multiple vibration modes.
- Numerical analyses on the sensitivity of the problem with respect to the link stiffness suggest that a limited number of arrangements of the elastic links per each panel are actually significant, namely (i) all the springs have the same stiffness, (ii) very weak stiffness for the external links, or (iii) very weak stiffness for the internal links. These considerations allow reducing the number of variables in the optimisation problem with respect to the case study shown in this work, e.g. considering only a single type of elastic spring for all links.

Future analyses will be carried out to study the effectiveness of DSFs as vibration absorber under wind excitation and for building layouts with irregularities both in plan and in elevation.

REFERENCES

[1] Housner GW, Bergman LA, Caughey TK, Chassiakos AG, Claus RO, Masri SF, Skelton RE, Soong TT, Spencer BF, Yao JTP. Structural control: past, present, and future. *Journal of Engineering Mechanics-Asce* sep 1997; **123**(9):897–971.

DOI: 10.1002/stc

[2] Den Hartog J. *Mechanical vibrations*. Dover Publications, 1947.

[3] Warburton GB. Optimum absorber parameters for various combinations of response and excitation parameters. *Earthquake Engineering & Structural Dynamics* may 1982; **10**(3):381–401.

[4] Ghosh A, Basu B. A closed-form optimal tuning criterion for TMD in damped structures. *Structural Control and Health Monitoring* jun 2007; **14**(4):681–692.

[5] Asami T, Nishihara O, Baz AM. Analytical Solutions to H_∞ and H_2 Optimization of Dynamic Vibration Absorbers Attached to Damped Linear Systems. *Journal of Vibration and Acoustics* 2002; **124**(2):284.

[6] Zuo L, Nayfeh S. Minimax optimization of multi-degree-of-freedom tuned-mass dampers. *Journal of Sound and Vibration* 2004; **272**(3-5):893–908.

[7] Casciati F, Giuliano F. Performance of Multi-TMD in the Towers of Suspension Bridges. *Journal of Vibration and Control* 2009; **15**(6):821–847.

[8] Moon KS. Dynamic interrelationship between technology and architecture in tall buildings. PhD Thesis, Massachusetts Institute of Technology 2005.

[9] Moon KS. Structural design of double skin facades as damping devices for tall buildings. *Procedia Engineering* 2011; **14**:1351–1358.

[10] Gratia E, De Herde A. Natural cooling strategies efficiency in an office building with a double-skin façade. *Energy and Buildings* 2004; **36**(11):1139–1152.

[11] Poirazis H. Double skin façades for office buildings: literature review. *Technical Report*, Lund University, Lund Institute of Technology, Lund 2004.

[12] Hensen J, Bartak M, Drkal F. Modeling and simulation of a double-skin façade system. *ASHRAE Transactions* 2002; **108 PART 2**(November):1251–1258.

[13] Park CS, Augenbroe G, Sadegh N, Thitisawat M, Messadi T. Real-time optimization of a double-skin façade based on lumped modeling and occupant preference. *Building and Environment* 2004; **39**(8 SPEC. ISS.):939–948.

[14] Høseggen R, Wachenfeldt BJ, Hanssen SO. Building simulation as an assisting tool in decision making. Case study: With or without a double-skin façade? *Energy and Buildings* 2008; **40**(5):821–827.

[15] Moon KS. Integrated Damping Systems for Tall Buildings. *Aei 2015*, 2015; 134–140.

[16] Moon KS. Integrated damping systems for tall buildings: tuned mass damper/double skin facade damping interaction system. *The Structural Design of Tall and Special Buildings* apr 2016; **25**(5):232–244.

[17] Samali B, Attard MM, Song C, Ngo T. Application of flexible facade systems in reducing the lateral displacement of concrete frames subject to seismic loads. *22nd Australian Conference on the Mechanics of Structures and Materials*, CRC Press/Balkema, 2013; 241–245.

[18] Fu TS. Double skin façades as mass dampers. *2013 American Control Conference*, IEEE, 2013; 4742–4746.

[19] Fu T, Zhang R. Integrating Double-Skin Façades and Mass Dampers for Structural Safety and Energy Efficiency. *Journal of Architectural Engineering* 2016; **22**(4):4016 014.

[20] Azad A, Ngo T, Samali B. Control of wind-Induced Motion of Tall Buildings Using Smart Façade Systems. *Electronic Journal of Structural Engineering* 2015; **14**(1):33–40.

[21] Azad A, Samali B, Ngo T, Nguyen C. Dynamic behaviour of flexible facade systems in tall buildings subjected to wind loads. *From Materials to Structures: Advancement through Innovation*. CRC Press, 2012; 431–435.

[22] Palmeri A, Barone G, Khetawat A. Passive control of building structures using double-skin facades as vibration absorbers. *2015 Proceedings of the Fifteenth International Conference on Civil, Structural and Environmental Engineering Computing*, 2015; 1–12.

[23] Spencer Jr BF, Christenson RE, Dyke SJ. Next generation benchmark control problem for seismically excited buildings. *Second World Conference on Structural Control* 1998; :1135–1360.

DOI: 10.1002/stc

[24] Salvi J, Rizzi E. Optimum tuning of tuned mass dampers for frame structures under earthquake excitation. *Structural Control and Health Monitoring* apr 2015; **22**(4):707–725.

[25] Kasinos S, Palmeri A, Lombardo M. Seismic response of combined primary-secondary structures with the component-mode synthesis method. *Proceedings of the Fifteenth International Conference on Civil, Structural and Environmental Engineering Computing*, Civil-Comp Press, Stirlingshire, UK, 2015; 1–20.

[26] Dowrick DJ. *Earthquake resistant design and risk reduction*. 2nd editio edn., Wiley, 2009.

[27] Ghosh A, Basu B. Effect of soil interaction on the performance of tuned mass dampers for seismic applications. *Journal of Sound and Vibration* jul 2004; **274**(3-5):1079–1090.

[28] Kennedy J. Particle swarm optimization. *Encyclopedia of Machine Learning* 2010; **46**(11):685–691.

[29] Ok E, Turkmen HS. Multi Objective Optimization of a Composite Drive Shaft using a Particle Swarm Algorithm. *2015 Proceedings of the Fifteenth International Conference on Civil, Structural and Environmental Engineering Computing*, 2015; 1–18.

[30] Leung AYT, Zhang H, Cheng CC, Lee YY. Particle swarm optimization of TMD by non-stationary base excitation during earthquake. *Earthquake Engineering and Structural Dynamics* jul 2008; **37**(9):1223–1246.

DOI: 10.1002/stc